Welding in the World
https://doi.org/10.1007/s40194-025-01923-9

RESEARCH PAPER

Welding of additively manufactured aluminium alloy components: challenges and mitigation strategies

Rafael Nunes[1,4,5] · Koen Faes[1] · Wim Verlinde[1] · Florian Probst[2] · Jens De Freese[2] · Julius Arnhold[3] · Wim De Waele[4] · Matthieu Lezaack[5] · Aude Simar[5]

Received: 25 September 2024 / Accepted: 22 December 2024

Abstract

Additive manufacturing (AM) has contributed to significant advances in the production of aluminium alloys, particularly through powder bed fusion (PBF) and directed energy deposition (DED) processes. However, joining of conventionally and additively manufactured components remains essential. This work focuses on the weldability of AM aluminium alloys using fusion and solid-state welding processes. The study analyses the microstructural evolution and mechanical properties, revealing a relationship between AM technology and joining process. In particular, fusion welding of PBF-laser beam (LB) produced aluminium alloys presented a significant limitation due to the high porosity level, especially in the weld zone near the PBF-LB base material. This region of high porosity, known as the pore belt region, has an enormous detrimental effect on the mechanical properties of the weld. This phenomenon is not observed when the welds are carried out by solid-state welding processes, which makes this group of welding processes very suitable for this type of material. On the other hand, fusion welding of aluminium alloys produced by wire arc additive manufacturing (DED-Arc or WAAM) exhibits a good stability and repeatability, analogous to conventional aluminium alloy welding practices. Rotational friction welding of DED-Arc-produced components presented an unexpected challenge. Due to the difference in ductility compared to conventionally manufactured parts, the process window for optimal process pressure was found to be very narrow and sensitive. The findings are confirmed by metallographic examination, hardness profile measurement, tensile and bend testing.

Keywords AlSi10Mg · EN AW-5083 · ER 5183 · Fusion welding process · Solid-state welding process · Weldability

Recommended for publication by Commission I - Additive Manufacturing, Surfacing, and Thermal Cutting

✉ Rafael Nunes
rafael.nunes@bil-ibs.be

Koen Faes
koen.faes@bil-ibs.be

Wim Verlinde
wim.verlinde@bil-ibs.be

Florian Probst
florian.probst.fp@gmail.com

Jens De Freese
defreese@slv-muenchen.de

Julius Arnhold
julius.arnhold@tum.de

Wim De Waele
wim.dewaele@ugent.be

Matthieu Lezaack
matthieu.lezaack@uclouvain.be

Aude Simar
aude.simar@uclouvain.be

1 Belgian Welding Institute, 9050 Ghent, Belgium

2 Gesellschaft Für Schweißtechnik International mbH - Niederlassung SLV München, Munich, Germany

3 TUM School of Engineering and Design, Technical University of Munich, Garching, Germany

4 Department of Electromechanical, Systems and Metal Engineering, Ghent University, 9050 Ghent, Belgium

5 Institute of Mechanics, Materials and Civil Engineering, Université Catholique de Louvain, 1348 Louvain La Neuve, Belgium

Published online: 20 January 2025

1 Introduction

Additive manufacturing (AM) technology has evolved steadily over the last few decades to overcome the challenges and the operational and financial drawbacks associated with conventional manufacturing processes. AM is a tool-less, near-net-shape production technology, based on three-dimensional (3D) model data [1]. This new type of processing has provided industries with unprecedented opportunities to produce metal components with complex free-form geometries, where such geometries are not achievable using conventional manufacturing techniques [2, 3]. Among the various types of AM processes for manufacturing of metallic components, two groups are highlighted for industrial applications: powder bed fusion (PBF) and directed energy deposition (DED) processes. While there are similarities between the two groups, such as the potential use of powder as feedstock material and the possibility of utilizing the same heat sources [4], like a laser or an electron beam, each group also has distinct advantages and limitations [5].

On the one hand, PBF processes are well known for their ability to produce extremely complex parts with high geometric accuracy but limited in size by the build chamber [6]. On the other hand, DED produces parts that are virtually unlimited in size, as the manufacturing process can still be mounted on a moving rail, but DED is limited regarding the geometrical complexity [7].

PBF produces parts by fusion of powder feedstock using a laser beam (PBF-LB [8]) or electron beam (PBF-EB [9]) as a heat source. The beam melts or sinters the material according to a defined scan strategy, to create features within a discrete layer. The chamber is purged, and a recoater arm provides a new layer of powder to be fused in a layer-by-layer process to create the final part. PBF-LB is also known as laser powder bed fusion (L-PBF) [10], selective laser melting (SLM™) [11], direct metal laser sintering (DMLS™) [12], and direct metal laser melting (DMLM) [13].

Directed energy deposition (DED) processes, as the name suggests, use directed energy in combination with a directed feed of material to be melted and solidified according to a specific deposition path strategy. In this case, the feed materials are usually in powder or wire form. DED-Arc is most referred to by academia and industry as wire arc additive manufacturing (WAAM). However, DED-Arc is not a single process but a group of AM processes that use an electric arc as heat source and wire as feedstock. In this sense, four individual DED-Arc processes are reported in literature. More specific the processes based on gas metal arc welding (GMAW), on gas tungsten arc welding (GTAW), on plasma arc welding (PAW), and on submerged arc welding (SAW) [14]. DED-Arc based on GMAW is most widely used; DED-Arc based on SAW is only seen in very specific applications.

Although there are several advantages and limitations associated with these two major AM groups (PBF and DED), such as the cost of equipment and raw materials and the level of industrial maturity, the most important selection criteria for the manufacture of aluminium parts are the dimensional printing limitations and the complexity of the desired part, as illustrated in Fig. 1.

However, despite the many advantages of the AM technology, it is not feasible to produce a complex product without conventional manufacturing processes, either for financial or operational reasons. In this way, the ability to join conventionally and additively manufactured components or parts represents a crucial step towards the future use and consolidation of conventional and additive manufacturing technologies. Despite the growing interest in AM technologies, there is still a significant lack of knowledge about joining of conventionally and additively manufactured components.

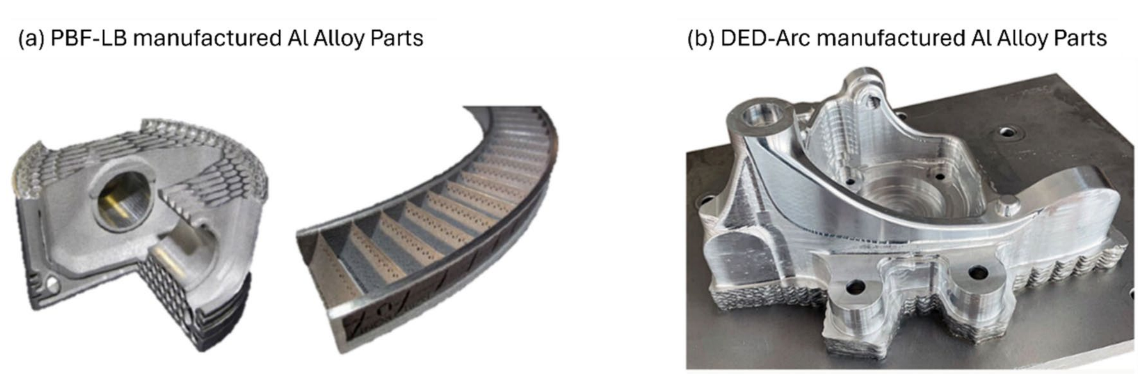

Fig. 1 Aluminium parts manufactured by PBF-LB (**a**) and DED-Arc (**b**) processes. At the left, ER 2024 and ER 6061 aluminium parts manufactured by Elementum 3D [15]. At the right, an ER 5183 aluminium part manufactured by Migal [16]

Even when considering the same (or very similar) chemical composition, the additive manufacturing processes of aluminium parts drastically increase the complexity of welding. As different AM processes produce different microstructures and mechanical properties, the weldability of these materials is also different. A common feature described by all authors who studied fusion welding of aluminium parts produced by PBF-LB is the significantly higher pore susceptibility compared to conventional materials of the same alloy. A significantly high porosity content after fusion welding has been found for the two typical aluminium alloys used in PBF-LB, i.e., AlSi10Mg [17–33] and AlSi12 [20, 34], especially in the weld zone (WZ) region near the PBF-LB base material, the so-called pore belt region [35].

In parallel with the high complexity of the process, there is an apparent lack of information on specific aspects of the weldability of AM aluminium alloys. The existing literature primarily focuses on feasibility studies, typically investigating a single alloy and welding process. This scarcity of quantitative data hinders comprehensive comparisons across different materials and joining techniques.

Through an extensive matrix of experiments using gas tungsten arc welding (GTAW), gas metal arc welding (GMAW), plasma arc welding (PAW), laser beam welding (LBW), friction stir welding (FSW), and rotary friction welding (RFW), this work provides an overview of the weldability of DED-Arc and PBF-LB manufactured aluminium alloys, highlighting the typical challenges to be overcome and the best selection of welding processes based on the involved parts.

2 Experimental methods and materials

2.1 Experimental methods

All welds were evaluated based on metallographic examination by optical microscope, hardness profile measurements, and tensile and bend testing. In addition to that, selected samples were evaluated by computed tomography (CT), scanning electron microscopy (SEM), and energy dispersive spectroscopy (EDS) for a deeper understating of specific findings.

The etching of the cross-sections for internal investigation was performed by HF for 10 s. The hardness HV10 measurements were carried out in the centre line of the plate thickness, with 2 mm between the indentations following the EN ISO 9015–1:2001 [36], as illustrated in Fig. 2.

For the mechanical characterization based on tensile and bend testing of the welds, samples perpendicular to the welding direction were extracted. Both sample extraction and mechanical testing were performed following the EN ISO 15614–2:2015 standard [37]. The design of the extracted tensile testing samples is shown in Fig. 3.

2.2 Base materials and filler metal

To investigate the weldability of additively manufactured aluminium alloy parts, a design of experiments (DOE) approach was employed. This DOE evaluated combinations of PBF-LB (AlSi10Mg) and DED-Arc (ER 5183) manufactured parts joined with conventionally manufactured EN AW-5083 H111 parts. As a reference, welds between conventionally manufactured aluminium alloy parts were also carried out using each of the welding processes evaluated. The chemical composition provided by certificate of the three selected materials is given in Table 1.

The microstructures of the three selected materials have completely different characteristics due to the different thermal cycles of their manufacturing processes. The microstructures in the vertical and horizontal directions are shown in Fig. 4. As a consequence of the different microstructures and chemical compositions, their mechanical properties are also different. The tensile strength of conventional EN AW-5083, DED-Arc ER 5183, and PBF-LB AlSi10Mg parts are 311 MPa, 288 MPa, and 436 MPa, respectively.

In the DED-Arc process, significant variations in material properties are expected between the vertical and horizontal directions due to slower cooling rates, columnar

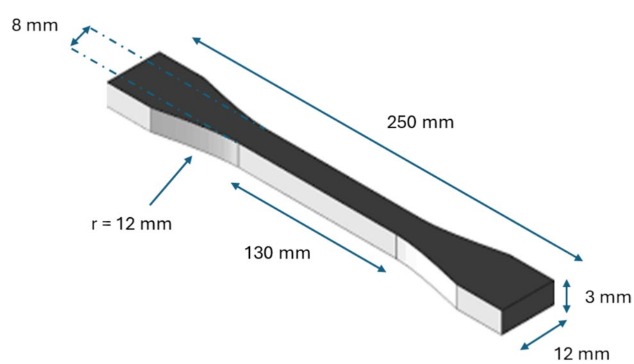

Fig. 3 Design of the extracted tensile testing sample

Fig. 2 Example of hardness HV10 measurements

Table 1 Chemical composition of conventionally manufactured EN AW-5083, DED-Arc manufactured ER 5183, and PBF-LB manufactured AlSi10Mg Al-alloys

Manufacturing process	Chemical composition in wt%										
	Al	Cu	Fe	Mg	Mn	Ni	Si	Cr	Ti	Zn	Zr
Conv-Cold Rolled EN AW-5083 H111	bal	0.05	0.36	4.7	0.7	-	0.19	0.11	0.02	0.01	-
DED-Arc ER 5183	bal	-	-	4.3–5.2	0.5–1.0	-	-	0.05–0.25	< 0.15	-	-
PBF-LB AlSi10Mg	bal	< 0.01	0.16	0.34	< 0,01	0.02	9.91	-	< 0.01	< 0.01	< 0.01

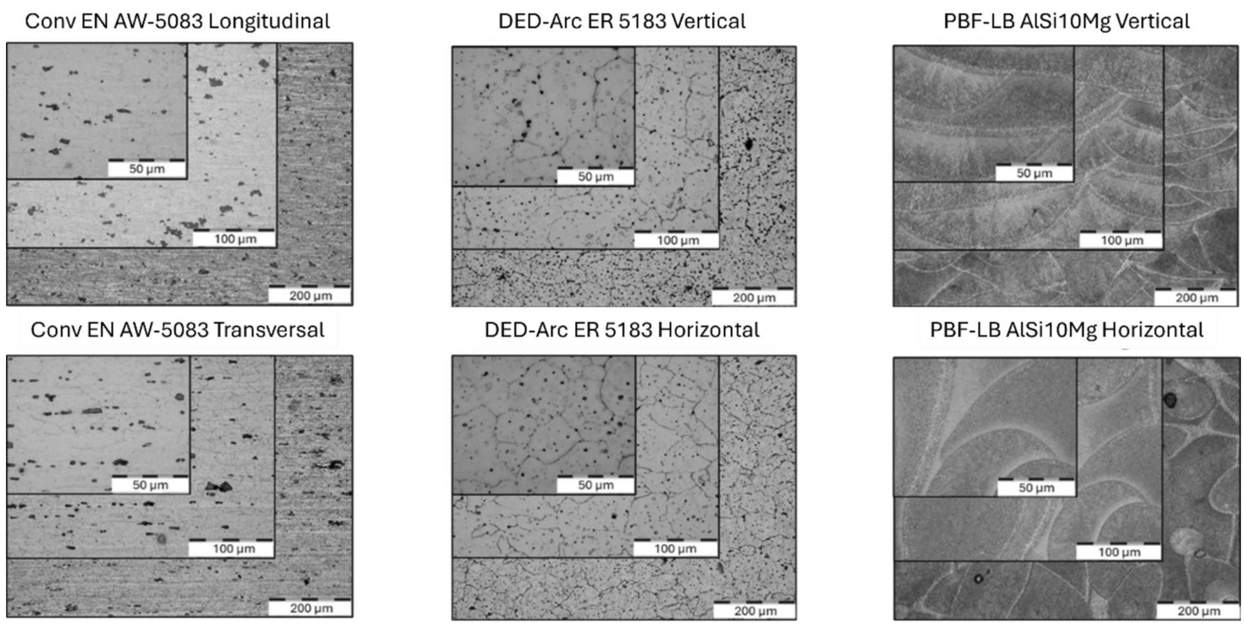

Fig. 4 Microstructures of conventionally (CONV) manufactured EN AW-5083, DED-Arc manufactured ER 5183, and PBF-LB manufactured AlSi10Mg parts in vertical (longitudinal and PB—parallel to build direction) and horizontal (transversal and PDD—parallel to deposition direction) directions

grain structures, and higher residual stresses. In contrast, PBF-LB generally exhibits less variation, owing to its finer microstructure and faster cooling rates [38]. Consequently, the DOE accounts for the direction of the extracted DED-Arc samples, categorizing them into vertical (parallel to the build direction) and horizontal (parallel to the deposition direction) orientations. The orientation of the extracted DED-Arc ER 5183 samples relative to the substrate is shown in Fig. 5.

As expected and observed by different authors [39, 40], there is a small difference in the tensile strength between DED-Arc PDD (291 MPa) and DED-Arc PBD (266 MPa). As the result does not represent a critical difference, the average value of 288 MPa was used to characterize this material, as previously described.

For all the welding processes using filler metal, e.g., GMAW, GTAW, and PAW, the ER 5356 wire of 1.2 mm of diameter was used as filler metal. The selection of the filler metal was made based on previous exploratory experiments. As typically used for welding of Al alloys, a shielding gas of Ar was used for the performing of all the fusion welding processes, e.g., GMAW, GTAW, PAW, and LBW.

2.3 Material combinations and design of experiment

The aim of the work is not only to evaluate the weldability of additively manufactured Al-alloy parts by a single welding process but to provide an overview and comparison of the weldability of these materials using different welding

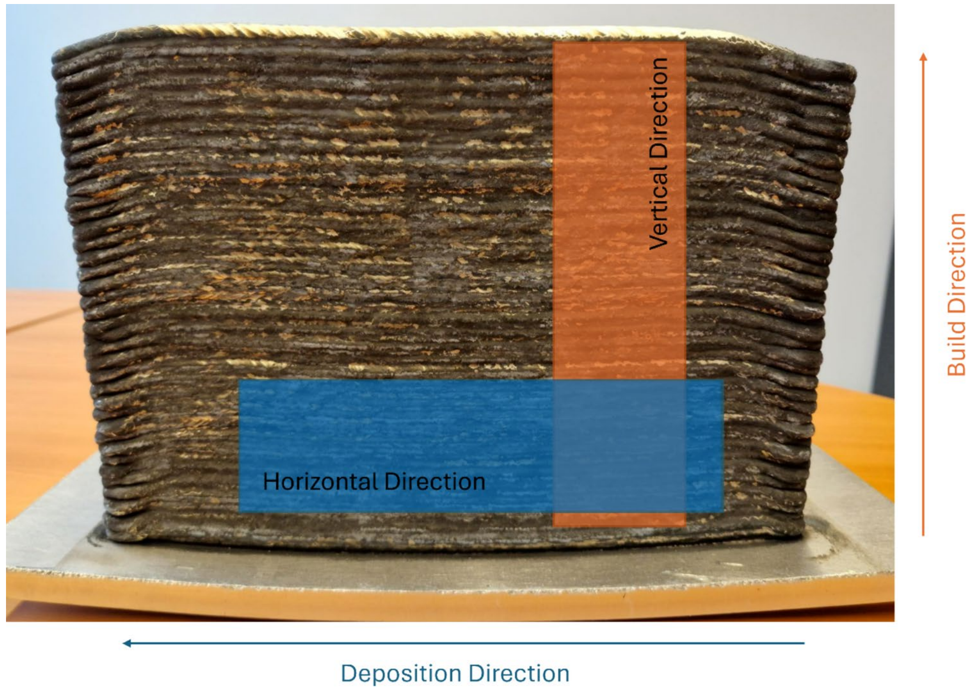

Fig. 5 Direction of the extracted DED-Arc ER 5183 samples with respect to the substrate

techniques. Among the selected dissimilar welding processes, GTAW, GMAW, PAW, and LBW are classified as fusion welding processes, while FSW and RFW are classified as solid-state welding processes.

Table 2 lists the material combinations and their respective optimized welding parameters used in each welded sample and the welding method applied.

Due to the limited amount of additively manufactured parts compared to the extensive DOE proposed, the joint design of Fig. 6 was used. RFW was the only welding process performed on tubular parts, while the others were performed on plates.

The welding processes GTAW, GMAW, and PAW all utilized the ER5356 filler metal with varying diameters: 2.4 mm, 1.2 mm, and 1.2 mm, respectively. As observed by Wu et al. [41], the use of the ER5356 filler metal resulted in enhanced weldability for additively manufactured Al-alloy parts. Besides these processes, LBW, FSW, and RFW were performed without filler metal.

3 Weldability investigations

In what follows, the welding experiments and their respective results and discussions are divided into two groups: fusion welding and solid-state welding processes. First, the results of the macrostructure and microstructure analyses are discussed. Second, the results of the mechanical analyses are discussed.

3.1 Macrostructure and microstructure analysis

After performing the welding tests, all samples were analysed based on metallographic examination. Figure 7 illustrates the welds performed by fusion welding processes.

Although the weldability of conventionally manufactured aluminium alloys is already considered lower compared to other materials due to the material intrinsic characteristics [42], it was possible to achieve welds without internal discontinuities using the four selected fusion welding processes. This result was achieved after exploratory tests to optimize the welding parameters. The welds involving the parts manufactured by DED-Arc achieved a similar satisfactory result. No pore-rich regions were found in the welds, as well as any other internal defects. The same results were found for the DED-Arc PDD and DED-Arc PBD parts. Because of the similarity in results, only one metallographic image is shown for each welding process.

As described in the literature, the weldability of Al-alloy parts manufactured by PBF-LB is extremely low when performed by fusion welding processes. During the experiments by GTAW, GMAW, and PAW, visual examination revealed

Table 2 Overview of the material combinations and their respective optimized welding parameters used in each welded sample

Welding process	Material A	Material B	Welding parameters			
			AVG current	AVG voltage	AVG wire feed speed	Welding speed
GMAW	Conv EN AW-5083	Conv EN AW-5083	64 A	16.9 V	4.3 m/min	28 cm/min
	Conv EN AW-5083	DED-Arc ER 5183 PDD	97 A	17.7 V	5.7 m/min	57 cm/min
	Conv EN AW-5083	DED-Arc ER 5183 PBD	97 A	17.7 V	5.7 m/min	57 cm/min
	Conv EN AW-5083	PBF-LB AlSi10Mg	72 A	16.9 V	4.5 m/min	28 cm/min
			AVG current	AVG voltage	Welding speed	
GTAW	Conv EN AW-5083	Conv EN AW-5083	90 A	13.0 V	8 cm/min	
	Conv EN AW-5083	DED-Arc ER 5183 PDD	90 A	13.0 V	10 cm/min	
	Conv EN AW-5083	DED-Arc ER 5183 PBD	90 A	13.0 V	10 cm/min	
	Conv EN AW-5083	PBF-LB AlSi10Mg	90 A	13.5 V	6 cm/min	
			AVG current	AVG voltage	AVG wire feed speed	Welding speed
PAW	Conv EN AW-5083	Conv EN AW-5083	110 A	18.1 V	1.1 m/min	18 cm/min
	Conv EN AW-5083	DED-Arc ER 5183 PDD	110 A	18.1 V	1.1 m/min	18 cm/min
	Conv EN AW-5083	DED-Arc ER 5183 PBD	110 A	18.1 V	1.1 m/min	18 cm/min
	Conv EN AW-5083	PBF-LB AlSi10Mg	110 A	18.1 V	1.1 m/min	18 cm/min
			AVG laser power	Welding Speed	Focus diameter	Wavelength
LBW	Conv EN AW-5083	Conv EN AW-5083	4.0 kW	720 cm/min	400 µm	1064 nm
	Conv EN AW-5083	DED-Arc ER 5183 PDD	4.0 kW	720 cm/min	400 µm	1064 nm
	Conv EN AW-5083	DED-Arc ER 5183 PBD	4.0 kW	720 cm/min	400 µm	1064 nm
	Conv EN AW-5083	PBF-LB AlSi10Mg	4.0 kW	720 cm/min	400 µm	1064 nm
			Rotational speed	Force	Welding speed	
FSW	Conv EN AW-5083	Conv EN AW-5083	1200 rpm	7.25 kN	20 cm/min	
	Conv EN AW-5083	DED-Arc ER 5183 PDD	1200 rpm	5.00 kN	20 cm/min	
	Conv EN AW-5083	DED-Arc ER 5183 PBD	1200 rpm	5.00 kN	20 cm/min	
	Conv EN AW-5083	PBF-LB AlSi10Mg	1200 rpm	7.25 kN	20 cm/min	
			Rotational speed	Friction pressure–time	Forge pressure–time	Holding pressure–time
RFW	Conv EN AW-5083	Conv EN AW-5083	1500 rpm	80 MPa-0.1 s	160 MPa-3.0 s	144 MPa-2.0 s
	Conv EN AW-5083	DED-Arc ER 5183 PDD	1500 rpm	70 MPa-0.1 s	105 MPa-3.0 s	126 MPa-2.0 s
	Conv EN AW-5083	PBF-LB AlSi10Mg	1500 rpm	70 MPa-0.1 s	140 MPa-3.0 s	126 MPa-2.0 s

a high porosity density region, termed the pore belt. This pore-rich region is observed in the WM near the fusion line in the PBF-LB parts, which has also been observed by other authors [17–34] and affects the joint quality [35].

Similar results were also found by Zhang et al. [18], who evaluated the difference in weldability of PBF-LB AlSi10Mg alloys using two different fusion welding processes: LBW and GTAW. Their results show a clear difference in porosity location and size distribution in the two welds. The pores in the LBW weld are more homogeneously distributed in the WM, whereas the pores in the GTAW weld are concentrated in the pore belt region. Due to its low heat concentration, arc welding allows a longer solidification time compared to laser welding, which allows the gas pores to rise and coalesce as they move upwards in the molten pool.

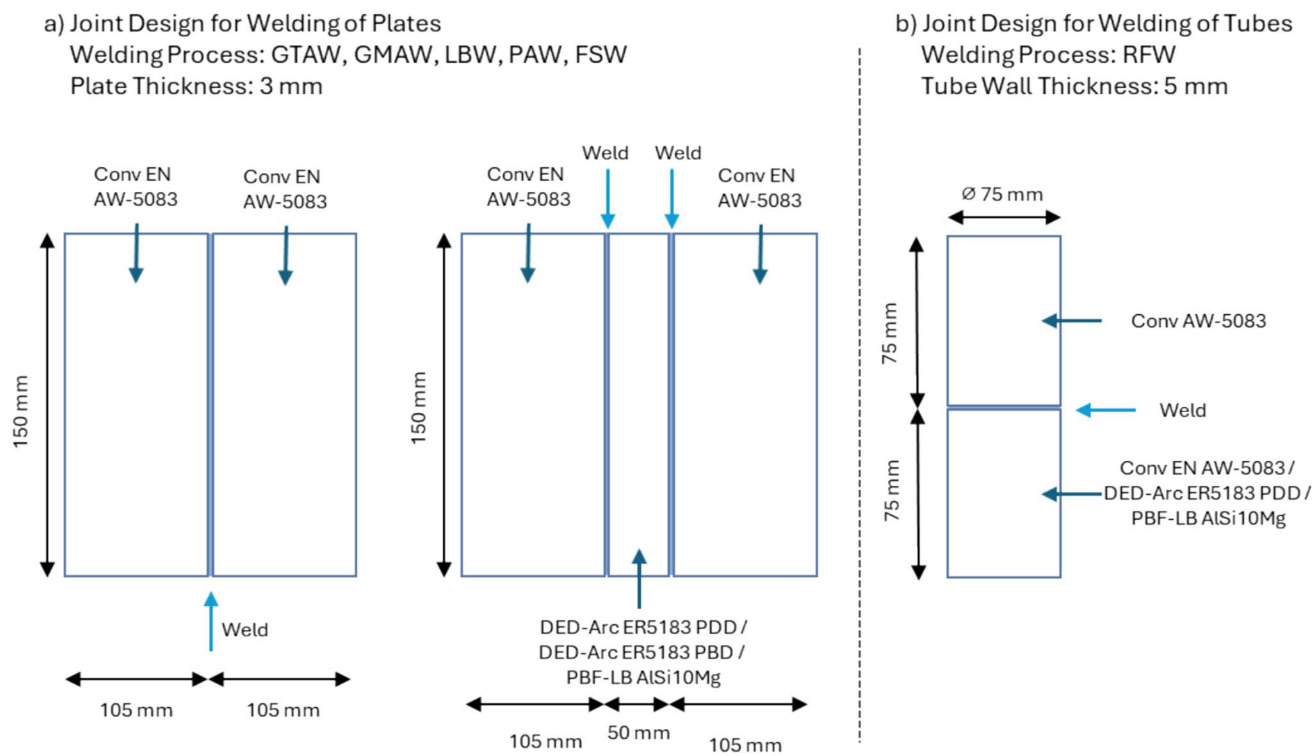

Fig. 6 Joint design for welding of **a** plates by GTAW, GMAW, LBW, PAW, and FSW processes and of **b** tubes by RFW process

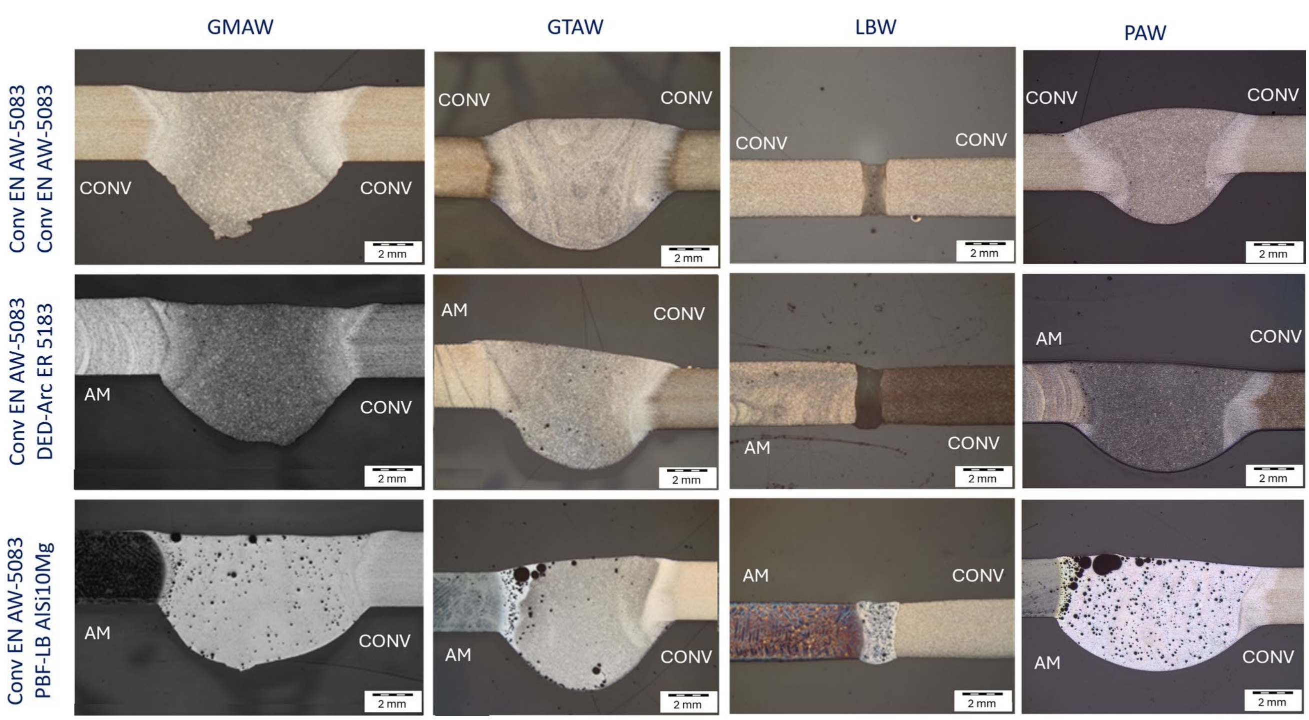

Fig. 7 Cross-section of welds performed by fusion welding processes GMAW, GTAW, LBW, and PAW

In addition to the thermal behaviour, the majority of research evaluating LBW has employed the autogenous technique, where no filler metal is added. Even when LBW is used with filler metal, the deposition rates are significantly lower than those possible with arc welding. The filler metal feed acts to push the porosity out, creating a denser region in the centre of the WM. In other words, it assists in the creation of the pore belt region. This behaviour is also observed in dissimilar welding involving PBF-LB manufactured Al alloy parts [17, 18], where the pore belt is formed in the FZ between the WM and the PBF-LB base metal. The described pore movement and coalescence in the arc welding and the autogenous beam welding processes can be observed in Fig. 8.

As illustrated in Fig. 9, computed tomography (CT) analysis reveals a continuous pore belt throughout the fusion zone of PBF-LB manufactured AlSi10Mg, irrespective of the welding process employed (GMAW, GTAW, or PAW).

Microstructural analysis of the fusion welds revealed two unexpected non-linear phenomena. Notably, the presence of α-Al dendrites surrounded by Si-eutectic phases resulted in localized hardening within the weld metal, see Fig. 10. Similar observations were made by different authors [23, 28, 29, 35].

In addition, a significant softening is observed in the HAZ, due to the spheroidization of Si in the PBF-LB heat-affected zone (HAZ), which can be observed in Fig. 11. Upon exposure to elevated temperatures below the melting point, the eutectic structure undergoes degradation, manifested by the spheroidization of the silicon-rich eutectic phase [42]. The absence of a eutectic structure, observed in both the conventionally manufactured EN AW-5083 and DED-Arc-manufactured ER 5183, explains the absence of this spheroidization phenomenon within their welds.

Solid-state welding offers a distinct advantage; due to the fact that these processes operate below the melting point of the alloys, welding does not alter the porosity level. Figure 12 shows the cross-sections of these welds. The reduced porosity leads to a stronger bond between the joined materials, improving the overall strength and integrity of the weld.

FSW produced excellent results for all material combinations, with no imperfections found in the welds. The achieved results are coherent to what is described in literature and observed by different authors [43–53]. Figure 13 illustrates the different regions and their respective microstructure aspects of the weld between conventionally manufactured EN AW-5083 and PBF-LB manufactured AlSi10Mg. The thermo-mechanically affected zone (TMAZ) presented a highly deformed microstructure, subjected to elevated temperatures and deformation, with grains elongated in an upward-flowing pattern, compressed around the nugget due to the tool's forging action. In this region, recrystallization and grain coarsening are absent, likely because of insufficient deformation strain. The Onion Rings (OR) were more pronounced presence on the advancing side (PBF-LB), due to the expectedly greater

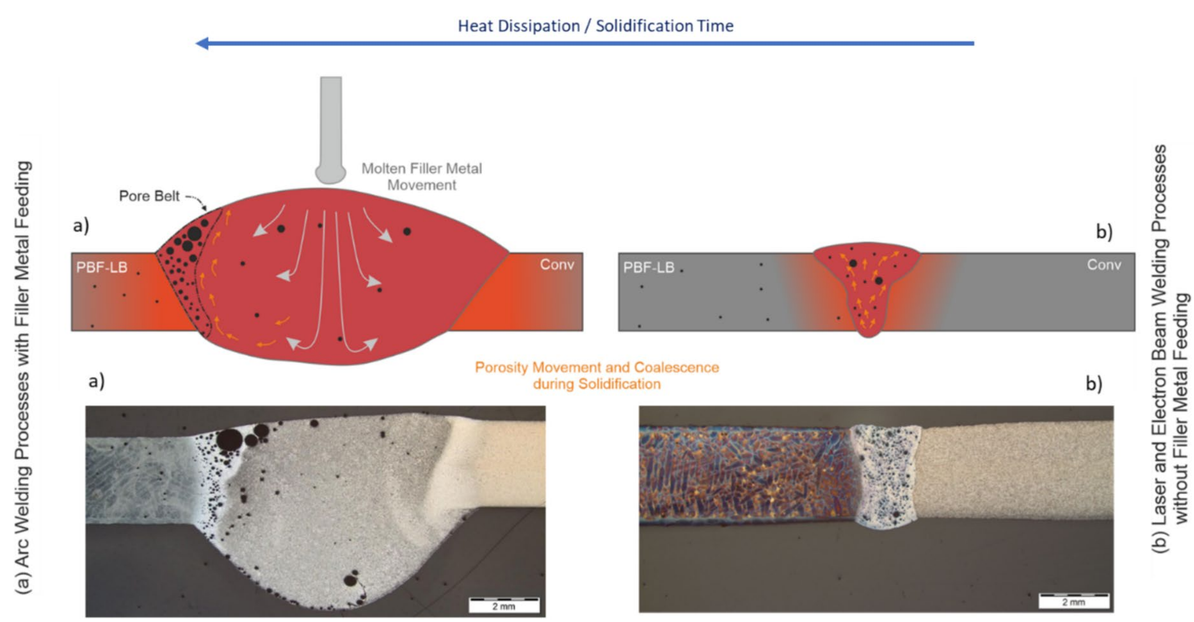

Fig. 8 Mechanism of pore movement and coalescence in the welds of PBF-LB manufactured Al alloys by arc welding (**a**) and laser and electron beam (**b**) welding processes [35]

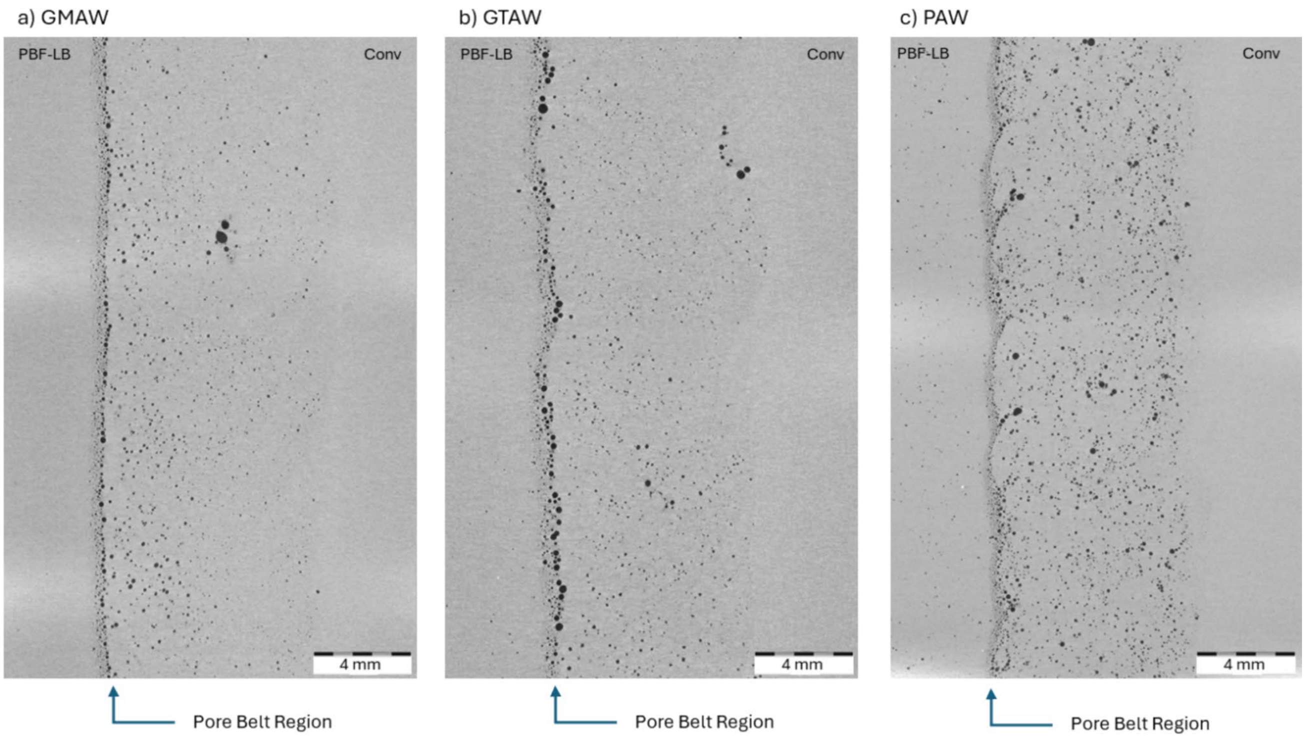

Fig. 9 Computed tomography of the top view of GMAW, GTAW, and PAW welds performed between conventionally manufactured EN AW-5083, and PBF-LB manufactured AlSi10Mg Al alloys, highlighting the presence of a continuous pore belt region in the length of the weld

plastic deformation on the advancing size during the welding process. In the centre of the weld zone, the weld nugget presented fine grain resulting from the significant plastic deformation, friction heating, and subsequent dynamic recrystallization.

An unexpected challenge arose during RFW welding of the DED-Arc-produced aluminium alloys. The weld between conventionally manufactured EN AW-5083 and DED-Arc manufactured ER 5183 parts showed to be very sensitive to

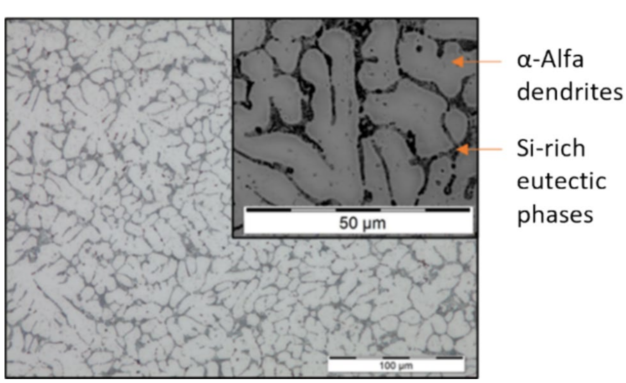

Fig. 10 Microstructure in the weld metal of fusion welded PBF-LB manufactured AlSi10Mg parts, highlighting the presence of α-Al dendrites surrounded by Si-eutectic phases

the process parameters involved in the RFW process, reducing the parameter window, and increasing the complexity of the process. During the parameter optimization experiments, a mere 8% difference in friction pressure was sufficient to transition from a condition of incomplete bonding to one resulting in fracture due to excessive pressure. The difficulty of friction welding lies in the significant difference of properties between the materials being joined, as observed by different authors [54–56]. The DED-Arc parts exhibit a higher ductility compared to conventional alloy EN AW-5083. The DED-Arc material has an elongation of at least 17% according to the filler material certificate, compared to a measured elongation of 8% for the conventional EN AW-5083 material. This difference in ductility creates challenges during friction welding.

The DED-Arc part, due to its high ductility, undergoes extensive plastic deformation throughout its volume. This means a large portion of the DED-Arc part deforms as a result of the forces and heat. This extensive internal deformation allows for the material to accommodate the relative movement between the workpieces without concentrating the plastic flow at the interface. Consequently, less material gets expelled as flash at the joint periphery. In contrast, due to its lower ductility, the conventionally manufactured EN AW-5083 material is limited to deform uniformly. As pressure and heat build up at the interface, the material struggles

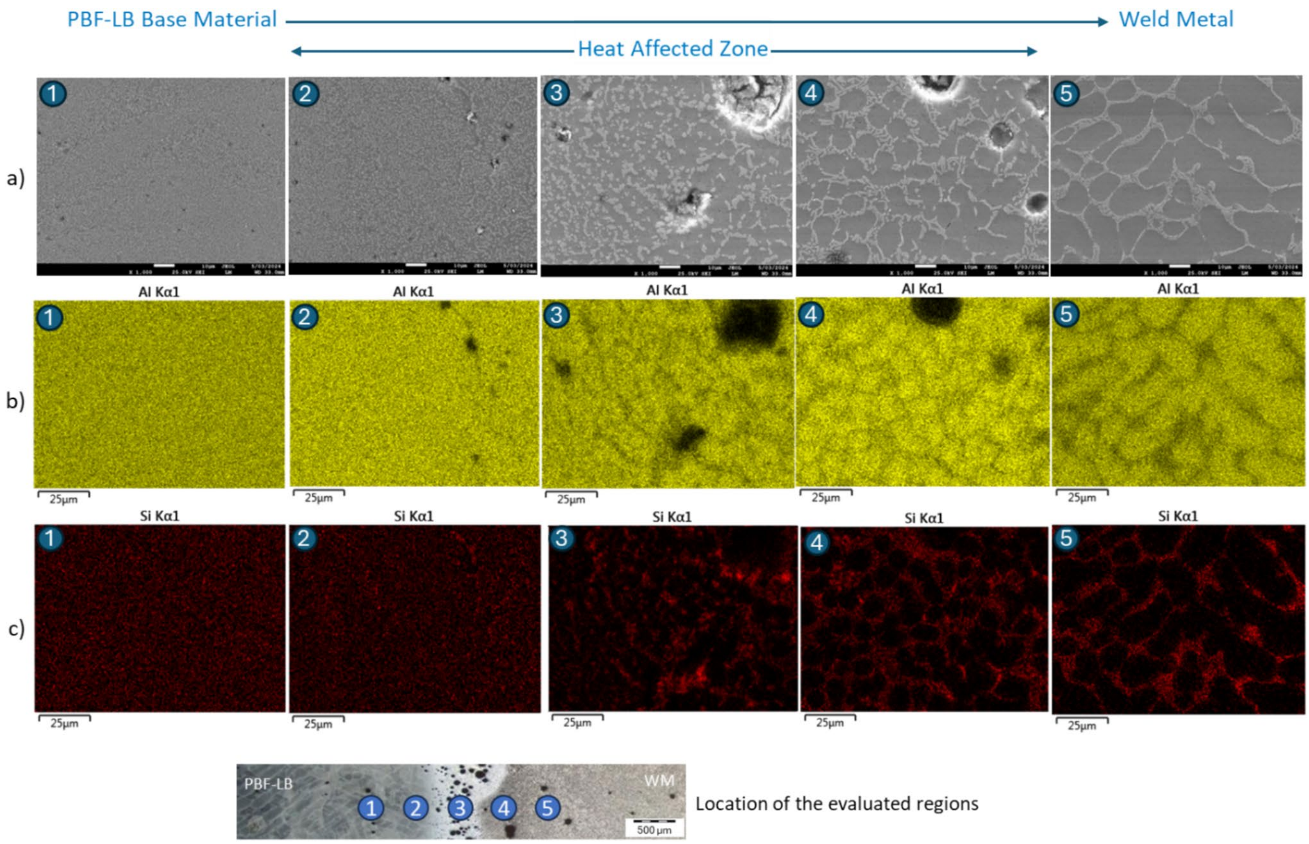

Fig. 11 Microstructure evolution of a fusion weld of PBF-LB AlSi10Mg highlighting the spheroidization of the Si in the PBF-LB heat affected zone, evidenced by **a** SEM analysis, **b** EDS mapping of the Al content, and **c** EDS mapping of the Si content

Fig. 12 Cross-sections of welds performed by the solid-state welding processes FSW and RFW

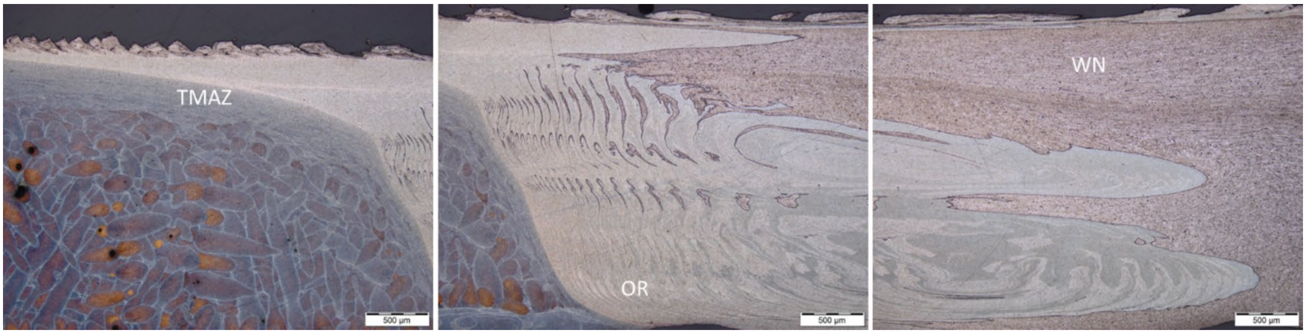

Fig. 13 Cross-section of a FSW weld between conventionally manufactured EN AW-5083 and PBF-LB manufactured AlSi10Mg, highlighting the TMAZ, OR, and WN zones

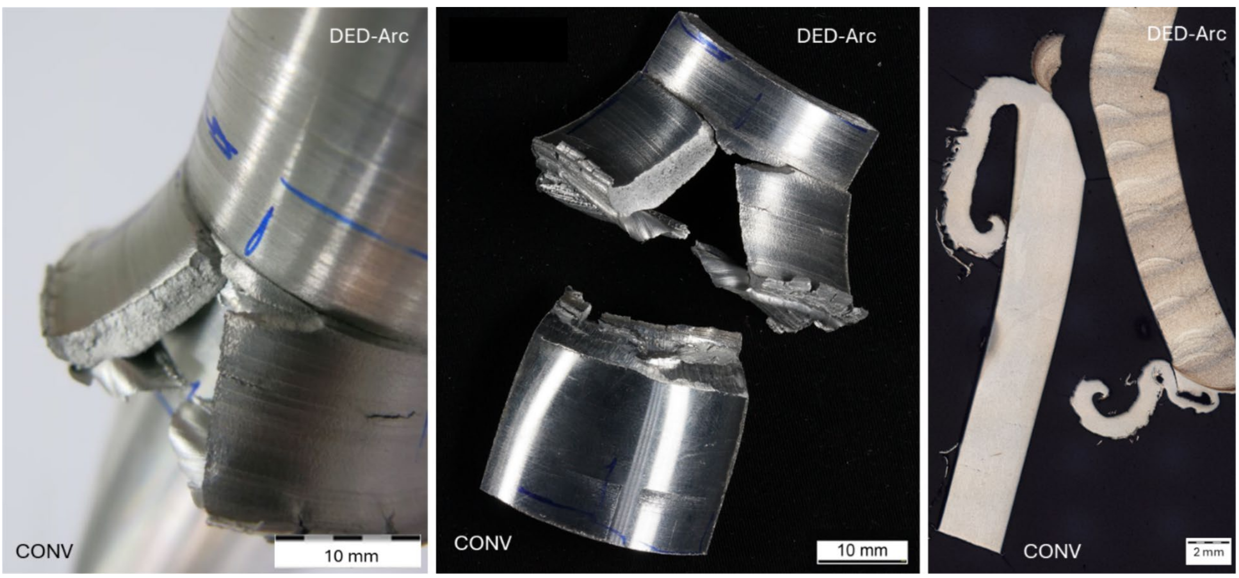

Fig. 14 Fracture during RFW process of conventionally manufactured EN AW-5083 to DED-Arc manufactured ER 5183 parts

to distribute the deformation throughout its volume. This localized deformation concentrates at the faying surfaces, where the workpieces touch, leading to the formation of a large flash (see Fig. 14). The large deformation of the DED-Arc part disrupted the formation of a proper weld, leading to a weak bond and complete failure.

The significant difference in ductility between DED-Arc ER 5183 and EN AW-5083 presents a challenge in finding optimal friction welding parameters. In this case, a delicate balance is required between the various process parameters that influence the heat input, i.e., friction pressure and friction time. Using a low friction pressure and/or a short friction, time can minimize the deformation of the highly ductile DED-Arc part. However, this approach increases the risk of a poor bond formation in the weld zone as it is shown in Fig. 15, because there is not enough heat to create a strong connection. In contrast, increasing the friction pressure and/or welding time will introduce more heat, promoting proper bonding. However, this approach on its turn significantly increases the deformation of the DED-Arc material.

In essence, the formation of a strong, high-quality weld relies on achieving a delicate equilibrium between the

Fig. 15 Incomplete joining region in the RFW weld of conventionally manufactured EN AW-5083 to DED-Arc manufactured ER 5183 parts

process parameters that influence the heat input. The process parameters need to be carefully chosen to limit the heat input in order to minimize the deformation of the DED-Arc part, while ensuring a sufficient heat input for a strong bond.

The used parameters for friction welding of the conventional materials involved a forge pressure twice as high as the friction pressure (respectively 70 and 140 MPa). For welding of EN AW-50853 to DED-Arc ER 5183, a different strategy was necessary. Instead of following the standard 2:1 ratio, the forge pressure was lowered to 1.5 times of the friction pressure (70 and 105 MPa respectively). The forging time was equal to 3 s. This aimed to reduce the overall pressure applied during the forging stage and to minimize excessive deformation of the DED-Arc part. The rotation speed was set at 1500 rpm for all welding experiments. The holding pressure, which is applied after the forging stage, remained set at 90% of the forge pressure, with a holding time of 2 s. This is a common practice in friction welding and ensures proper consolidation of the joint during the final stage.

3.2 Mechanical properties

The dissimilar welds between conventionally manufactured EN AW-5083 alloy and either its counterpart (EN AW-5083) or DED-Arc-produced ER 5183, fabricated using both the fusion and solid-state welding processes, demonstrate a remarkable stability and consistency in terms of hardness. The measurements are illustrated in Figs. 16 and 17, respectively. The centre images in Figs. 16, 17, and 18 illustrate the general hardness evolution of the respective material combination by all welding processes, showing the minimum and maximum reached levels.

On the other hand, a different behaviour is observed in the hardness profiles of the welds between conventionally manufactured EN AW-5083 alloy and PBF-LB AlSi10Mg manufactured parts, as shown in Fig. 18.

The different hardness evolution of the welds between conventionally and PBF-LB manufactured Al alloys is clearly observed by the fusion and solid-state welding

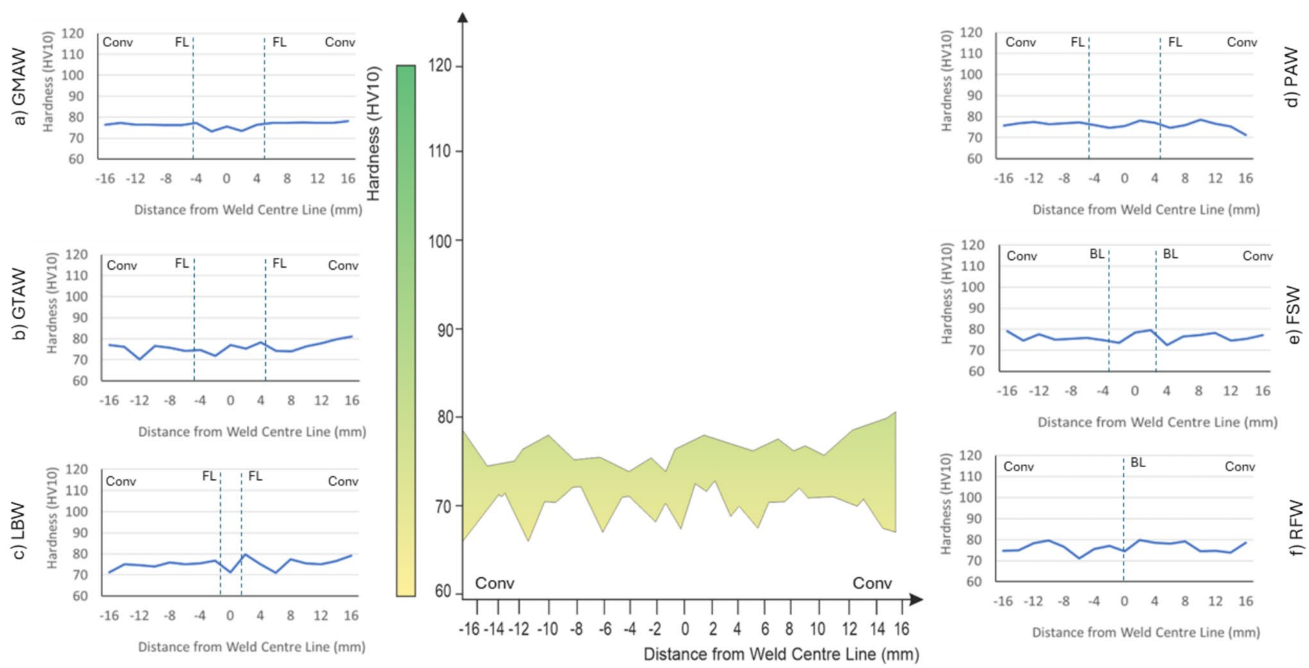

	Material Combination: Conv AW 5083 + Conv AW 5083																
	Hardness HV10 - Distance from Weld Centre Line (mm)																
	-16	-14	-12	-10	-8	-6	-4	-2	0	2	4	6	8	10	12	14	16
a) GMAW	76.5	77.3	76.5	76.5	76.3	76.2	77.2	73.2	75.6	73.5	76.4	77.3	77.3	77.5	77.3	77.4	78.1
b) GTAW	77.0	76.2	70.3	76.6	75.7	74.3	74.6	72.0	77.1	75.3	78.4	74.3	74.0	76.3	78.0	79.9	81.2
c) LBW	71.2	75.2	74.6	74.0	76.0	75.1	75.6	76.8	71.2	79.8	75.2	71.1	77.4	75.6	75.0	76.5	79.2
d) PAW	75.7	76.8	77.4	76.4	76.9	77.3	76.0	74.6	75.6	78.2	77.0	74.6	75.9	78.5	76.6	75.4	71.2
e) FSW	79.2	74.6	77.7	75.1	75.6	75.9	74.8	73.6	78.4	79.6	72.6	76.5	77.1	78.2	74.6	75.6	77.1
f) FRW	74.8	74.9	78.4	79.6	76.6	71.2	75.6	77.1	74.6	79.8	78.6	78.1	79.3	74.6	74.7	73.8	78.6

Fig. 16 Hardness profile of welds performed by GMAW, GTAW, LBW, PAW, FSW, and RFW between conventionally manufactured EN AW-5083 and conventionally manufactured EN AW-5083 aluminium alloy parts

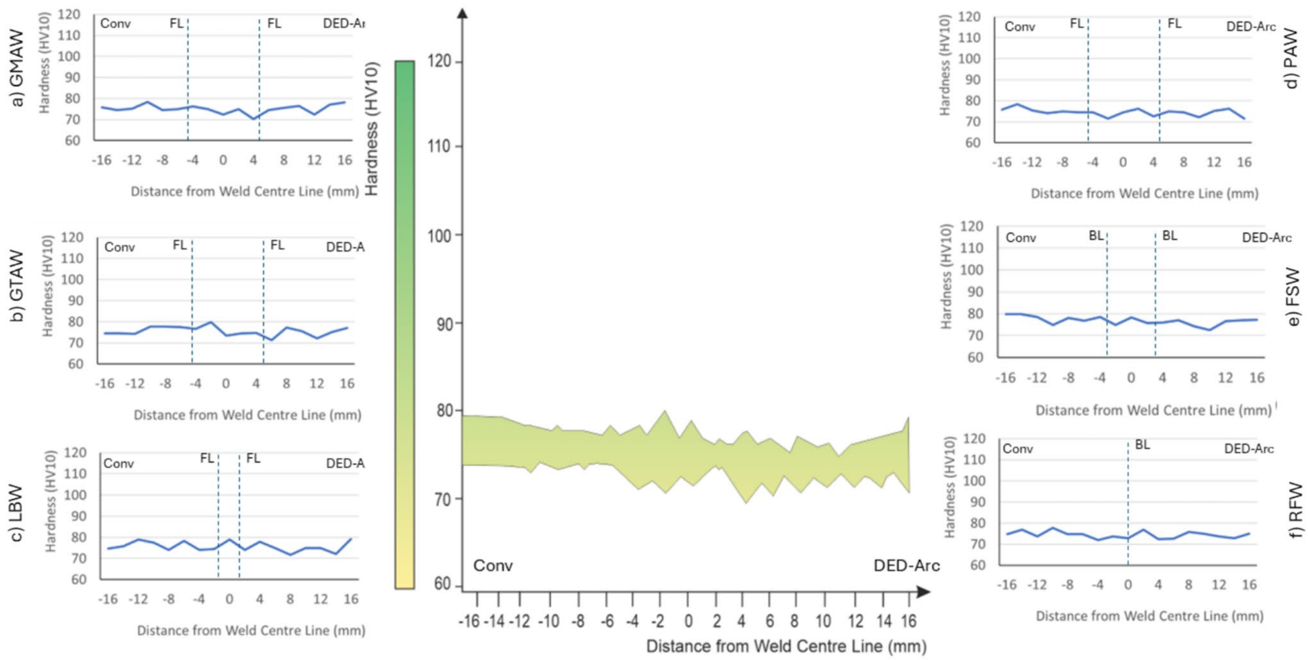

	Material Combination: Conv AW 5083 + WAAM ER 5183																
	Hardness HV10 - Distance from Weld Centre Line (mm)																
	-16	-14	-12	-10	-8	-6	-4	-2	0	2	4	6	8	10	12	14	16
a) GMAW	75.8	74.6	75.1	78.3	74.6	75.0	76.3	74.9	72.3	75.0	70.3	74.5	75.6	76.5	72.3	77.1	78.1
b) GTAW	74.6	74.5	74.2	77.8	77.7	77.4	76.6	79.8	73.5	74.6	74.8	71.2	77.2	75.6	72.1	75.2	77.1
c) LBW	74.6	75.8	78.9	77.4	74.1	78.4	74.1	74.4	78.9	74.1	77.8	74.9	71.6	74.8	74.9	72.1	79.2
d) PAW	75.8	78.4	75.4	74.1	74.9	74.6	74.5	71.5	74.6	76.3	72.6	74.9	74.5	72.1	75.2	76.2	71.6
e) FSW	79.8	79.8	78.4	74.9	78.1	76.8	78.4	74.9	78.2	75.8	76.0	77.1	74.3	72.6	76.5	77.1	77.2
f) FRW	74.8	77.0	73.8	77.8	74.8	74.8	71.9	73.8	72.9	77.0	72.4	72.6	75.9	74.9	73.6	72.8	74.9

Fig. 17 Hardness profile of welds performed by GMAW, GTAW, LBW, PAW, FSW, and RFW between conventionally manufactured EN AW-5083 and DED-Arc manufactured ER 5183 aluminium alloy parts

processes. From one side, the hardness evolution of the fusion welded (GMAW, GTAW, LBW, and PAW) presents two regions of interesting behaviours, the hardness in the WM, and the softening in the HAZ of the PBF-LB base material. Both behaviours are, as discussed in the previous sections, caused by the presence of α-Al dendrites surrounded by Si-eutectic phases and by the spheroidization of the Si-eutectic phases, respectively.

As expected, the tensile properties of the welds were significantly impacted by the presence of the pore belt regions in the fusion welded samples by GMAW, GTAW, and PAW. Although disperse, the high porosity level in the LBW welds had a similar impact on the tensile strength. The ultimate tensile strength of all welds is shown in Fig. 19.

It is important to mention that due to the obvious inhomogeneous characteristics of both materials and weld, the results from tensile testing should not be treated and compared as standard ultimate tensile strength. For this reason, the resulted value is highlighted as "Ultimate Tensile Strength * (MPa)".

Due to the different strength properties of the different materials, specific strength requirements for each material combination were stipulated, following the EN ISO 15614–2:2005 standard [37]. This standard requires that the welded test specimens should have a tensile strength equal to or exceeding the minimum specified strength of the base material. For dissimilar metal joints, the tensile strength should at least be equal to the minimum specified tensile strength of the base material with the lowest tensile strength (conventionally manufactured EN AW-5083). In Fig. 19, the columns with dashed fillings correspond to the weld conditions where the acceptance criteria were

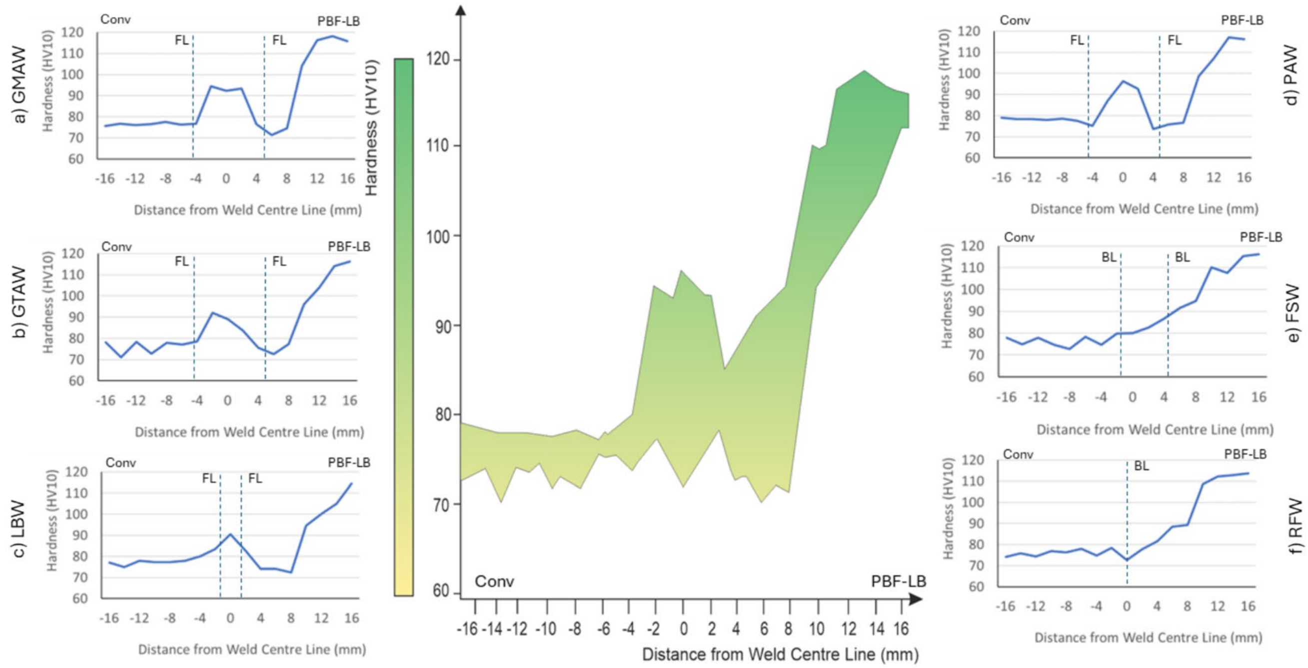

	Material Combination: Conv AW 5083 + PBF-LB AlSi10Mg																
	Hardness HV10 - Distance from Weld Centre Line (mm)																
	-16	-14	-12	-10	-8	-6	-4	-2	0	2	4	6	8	10	12	14	16
a) GMAW	75.6	76.6	76.0	76.5	77.5	76.2	76.6	94.4	92.3	93.4	76.4	71.3	74.5	104.0	116.2	118.2	115.9
b) GTAW	78.2	71.2	78.4	72.8	78.0	77.2	78.5	92.0	89.0	83.7	75.5	72.6	77.3	96.1	104.0	114.1	116.3
c) LBW	77.1	74.9	77.9	77.3	77.4	77.9	80.0	83.5	90.5	82.7	74.1	74.0	72.3	94.6	100.2	105.1	114.5
d) PAW	79.1	78.4	78.4	78.0	78.5	77.5	75.1	87.1	96.3	92.7	73.6	75.8	76.6	98.6	107.2	117.1	116.3
e) FSW	77.8	74.9	77.8	74.6	72.8	78.3	74.6	79.8	80.1	82.6	86.7	91.5	94.8	110.1	107.6	115.2	116.2
f) FRW	74.2	75.9	74.4	77.0	76.4	77.9	74.8	78.4	72.7	77.7	81.6	88.4	89.4	108.6	112.3	112.9	113.8

Fig. 18 Hardness profile of welds performed by GMAW, GTAW, LBW, PAW, FSW, and RFW between conventionally manufactured EN AW-5083 and PBF-LB manufactured AlSi10Mg aluminium alloy parts

not reach, while the solid columns without dashed fillings correspond to the tests with satisfactory results. Process parameter optimisation ensured that all welds of the conventional materials achieved satisfactory tensile test results, exceeding the standard's minimum requirements. The PAW welds were an exception to this, demonstrating a variable performance.

Although the GMAW welds performed with optimized parameters reached an acceptable value for the tensile strength, the bend test results of all fusion welds were not fulfilling the requirements specified in EN ISO 15614–2:2005 [37], as shown in Fig. 20. According to this standard, specimens must not exhibit any imperfections greater than 3 mm when bent to an angle equal to 180°.

By analysing the fracture location of the bend test samples, it was observed that the failure of the fusion welded samples always occurred at the same location (Fig. 21), in the pore belt region, which represents the critical region for the weld quality.

Evaluation through tensile and bend testing revealed that fusion welding processes did not negatively impact the weldability of DED-Arc-manufactured parts. In fact, these welds achieved similar strength and ductility values as those observed in welds of conventionally manufactured parts. However, metallographic examination identified one exception, i.e., rotational friction welding. In this case, the significant difference in ductility between the DED-Arc material and the conventional joining partner creates a zone with defects within the weld, compromising its performance.

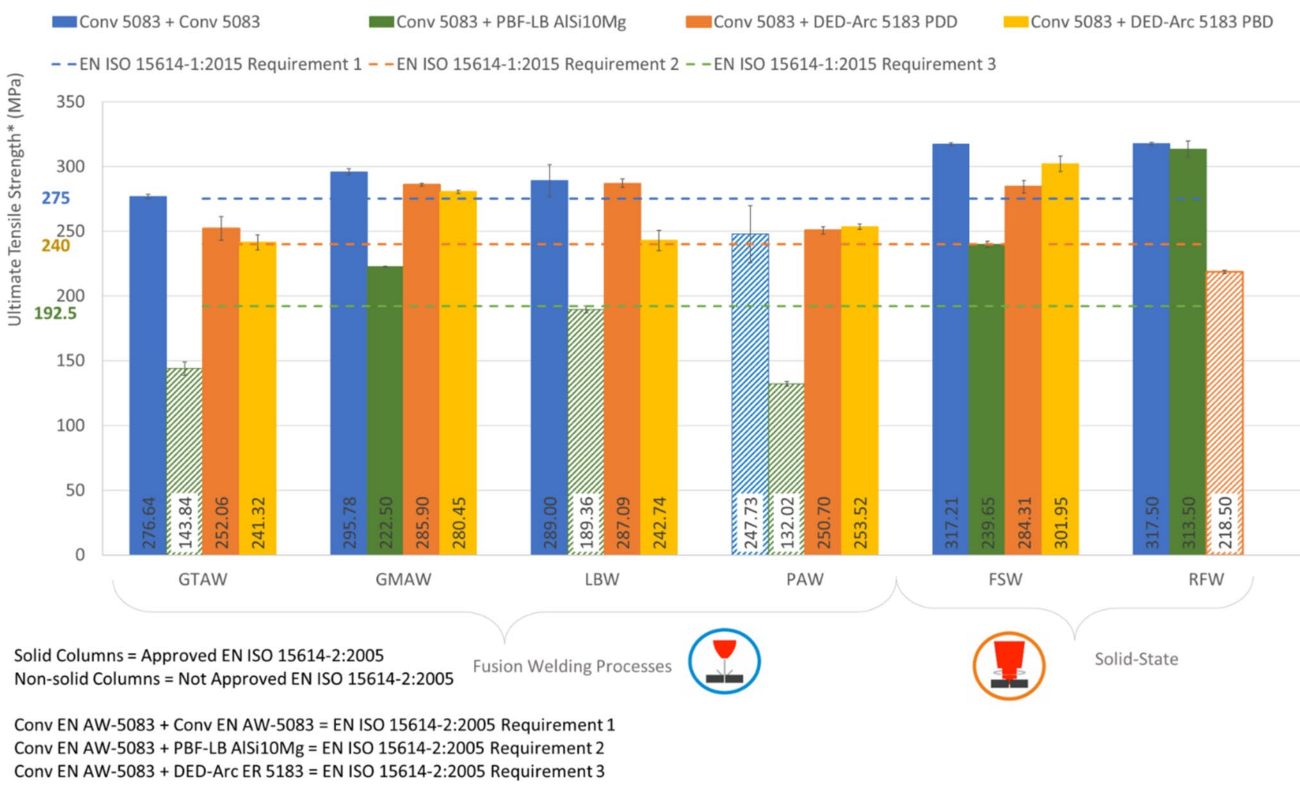

Fig. 19 Ultimate tensile strength of all material combinations joined through fusion and solid-state welding processes

	Welding Process	Material A	Material B	Bend Testing Result*
Fusion Welding Processes	GMAW	Conv EN AW-5083	Conv EN AW-5083	Approved
		Conv EN AW-5083	PBF-LB ALSi10Mg	Not Approved
		Conv EN AW-5083	DED-Arc ER 5183	Approved
	GTAW	Conv EN AW-5083	Conv EN AW-5083	Approved
		Conv EN AW-5083	PBF-LB ALSi10Mg	Not Approved
		Conv EN AW-5083	DED-Arc ER 5183	Approved
	LBW	Conv EN AW-5083	Conv EN AW-5083	Approved
		Conv EN AW-5083	PBF-LB ALSi10Mg	Not Approved
		Conv EN AW-5083	DED-Arc ER 5183	Approved
	PAW	Conv EN AW-5083	Conv EN AW-5083	Approved
		Conv EN AW-5083	PBF-LB ALSi10Mg	Not Approved
		Conv EN AW-5083	DED-Arc ER 5183	Approved
Solid-State Welding Processes	FSW	Conv EN AW-5083	Conv EN AW-5083	Approved
		Conv EN AW-5083	PBF-LB ALSi10Mg	Approved
		Conv EN AW-5083	DED-Arc ER 5183	Approved
	RFW	Conv EN AW-5083	Conv EN AW-5083	Approved
		Conv EN AW-5083	PBF-LB ALSi10Mg	Approved
		Conv EN AW-5083	DED-Arc ER 5183	Not Approved

* EN ISO 15614-2:2005

Fig. 20 Bend test results of all material combinations joined through fusion and solid-state welding processes

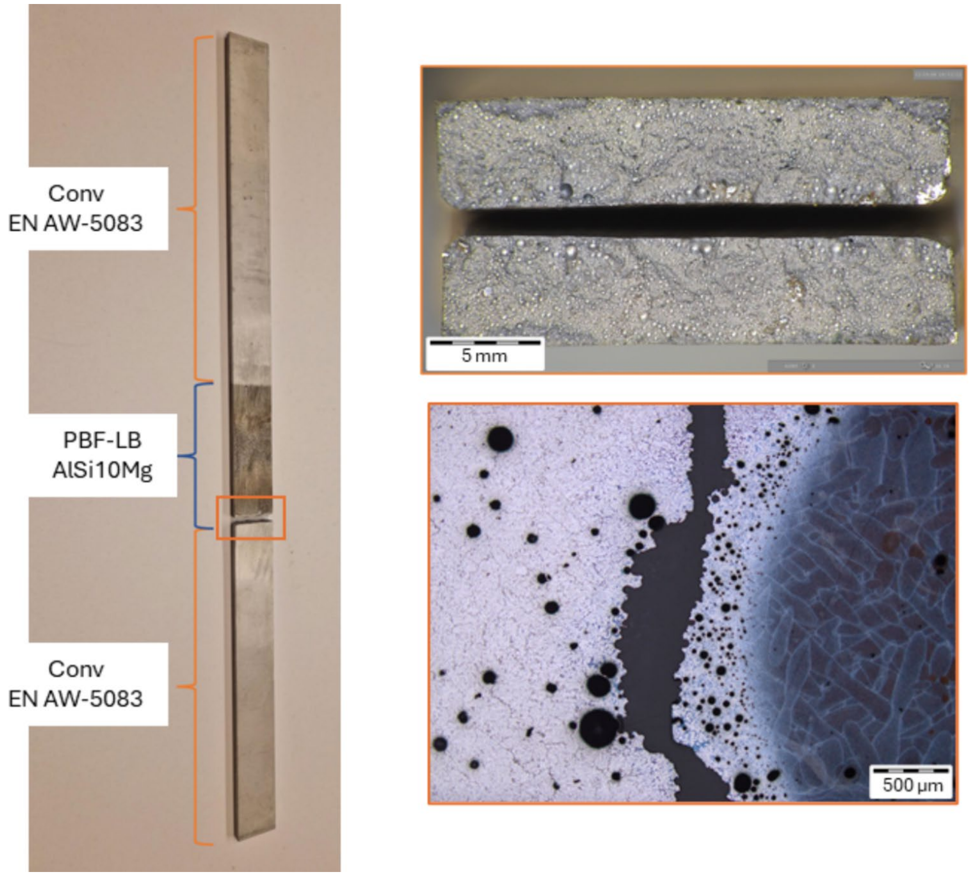

Fig. 21 Typical fracture location in the bend tested sample manufactured by PBF-LB and welded by fusion welding processes, evidencing the effect of the pore belt region on the location of fracture

3.3 Understanding the porosity in the welds of PBF-LB Al alloys

The high porosity levels found in the fusion welds, as well as the formation of the pore belt region, is clearly linked to the PBF-LB manufacturing process. As observed and suggested by different authors [35], it is unlikely that the porosity can be entirely avoided by optimisation of the welding parameters. Three main factors contribute to this observation.

The first factor is a main difference between PBF-LB and DED-Arc, which is the mechanism used to introduce the feedstock material for building the layers. PBF-LB utilizes a powder feedstock with a much higher surface area to volume ratio compared to the wire used in DED-Arc. This difference in feedstock material has a significant impact on the porosity levels in the resulting welds. As demonstrated by Griffiths et al. [17], welds of PBF-LB aluminium alloys can exhibit approximately 10 times higher porosity levels compared to welds of DED-Arc aluminium alloy. This significant difference highlights the impact of the chosen feedstock material on the quality of the final weld. Besides the filler material form itself, the powders used for PBF-LB process are typically produced via gas atomization, which normally results in powder with higher porosity level compared to the other production techniques, such as water or centrifugal atomization. This is primarily due to the rapid solidification and cooling rates during gas atomization, which often leads to the formation of fine, porous powders [57].

The second factor is the consequence of surface oxidation on reused and aged powder [58]. During handling and storage, powder particles can develop a thin oxide layer on their surface. While minimal oxidation might be tolerable, repeated reuse of powder can significantly deteriorate this issue. Partially melted powder particles are typically captured and sieved for potential reuse in subsequent builds. However, these reused particles may have undergone significant changes. The laser melting process itself can further oxidize the powder particles. Reusing them exposes them to additional heat cycles, potentially leading to a thicker and more detrimental oxide layer. The initial melting process can alter the size and shape (granulometry and morphology) of the powder particles. Reusing these particles can lead to inconsistencies in the powder bed, potentially affecting laser absorption and melt pool dynamics. The combined effect of increased oxidation altered granulometry and potentially changed morphology can significantly impact the quality of PBF-LB builds.

Research by Fedina et al. [58] provides evidence for the detrimental effects of powder reuse on the laser absorbance, a critical parameter in PBF-LB. Their findings indicate that reusing AlSi10Mg powder can lead to a significant decrease in laser absorbance, potentially by as much as 15%. Laser absorption plays a crucial role in the PBF-LB process. The laser beam melts the powder particles by transferring its energy. However, if the powder absorbs less energy due to oxidation or other factors, complete melting becomes difficult. Insufficient laser absorption can lead to partially melted particles within the powder bed. These unmelted regions can act as weak points or create voids within the final structure, increasing porosity.

The third and last factor contributing to the formation of pores in the PBF-LB manufactured aluminium alloy parts, and consequently in the welds of such parts, is that most of commercial equipment controls and monitors its inert atmosphere based on O_2 content, and not by creating a vacuum and then filling the chamber with Ar. This approach introduces the risk of hydrogen accumulation within the chamber, potentially leading to its absorption by the deposited material.

4 Conclusions

Welding of additively manufactured components plays a crucial role to allow versatile manufacturing. Additive manufacturing allows for the creation of complex geometries and near-net-shaped components. However, achieving the final desired shape often requires the use of additional manufacturing techniques like machining, finishing and welding. By joining additively manufactured parts through welding, higher design freedom, improved material utilisation, and an enhanced functionality for complex components can be achieved.

Regarding additively manufactured aluminium alloys, the biggest challenge is fusion welding of PBF-LB manufactured parts. Due to the formation of a large amount of pores, the mechanical properties of the welds are significantly impacted and reduced. A specific region, called the pore belt region, is present in the welds executed by GMAW, GTAW, and PAW processes. Based on the presented results and on literature, it is very unlikely that these imperfections can be overcome by parameters optimisation. In contrast to the observed issues with fusion welding of PBF-LB AlSi10Mg, solid-state welding yielded positive results, evident by the lack of internal imperfections.

DED-Arc manufactured ER 5183 components demonstrated excellent weldability for various fusion welding processes. These welds achieved mechanical properties and hardness profiles comparable to those obtained when welding conventionally manufactured AW EN-5083 materials. However, the rotary friction welding process presented the only significant challenge for joining DED-Arc-manufactured ER 5183. This is due to the difference in ductility between the DED-Arc material and the conventional joining partner.

As observed by the achieved results, the additive manufacturing process has a large impact on the weldability of the parts. Due to the different thermal cycles and the different feedstock materials used, the microstructure and consequently the mechanical properties and weldability of the manufactured parts also present different characteristics. The selection of a suitable welding process should therefore prioritize compatibility with the specific additive manufacturing technique used for the components.

Funding The presented results and discussions on the weldability of additively manufactured aluminium alloys were achieved during the COAMWELD project: “Advanced metal components through optimal combination of additive manufacturing and welding techniques,” funded by VLAIO (Flanders Innovation and Entrepreneurship) under Grant Agreement HBC.2020.2994.

Declarations

Conflict of interest The authors declare no competing interests.

References

1. Nunes R, Vandermeiren N, Verlinde W, Boruah D, Motte R, De Waele W (2023) A benchmark of mechanical properties and operational parameters of different steel filler metals for wire arc additive manufacturing. Int J Adv Manufact Technol 12:599–613. https://doi.org/10.1007/s00170-023-11520-z
2. Vafadar A, Guzzomi F, Rassau A, Hayward K (2021) Advances in metal additive manufacturing: a review of common processes, industrial applications, and current challenges. Applied Sci. 11(3). https://doi.org/10.3390/app11031213
3. Rasiya G, Shukla A, Saran K (2021) Additive manufacturing—a review. Mater Today: Processing. 47:6896–6901. https://doi.org/10.1016/j.matpr.2021.05.181
4. ASTM ISO (2022) Standard Terminology for additive manufacturing: general principles—fundamental and vocabulary, Astm. Org.https://www.astm.org/Standards/ISOASTM52900.htm. Accessed 4 Sep 2024
5. Gradl PR, Tinker DC, Park A, Mireles OR, Garcia M, Wilkerson RP, Mckinney C (2022) Robust metal additive manufacturing process selection and development for aerospace components. J Mater Eng Perform 31:6013–6044. https://doi.org/10.1007/s11665-022-06850-0
6. Singh DD, Mahender T, Reddy AR (2021) Powder bed fusion process: a brief review. MaterToday: Proceed V 46:350–355. https://doi.org/10.1016/j.matpr.2020.08.415
7. Ahn DG (2021) Directed Energy Deposition (DED) Process: state of the art. Int J of Precis Eng and Manuf-Green Tech 8:703–742. https://doi.org/10.1007/s40684-020-00302-7
8. Lasagni F, Galleguillos C, Herrera M, Sataolaya J, Hervas D, Gonzales S, Perinan A (2022) On the processability and mechanical behavior of Al–Mg–Sc alloy for PBF-LB. Prog Addit Manuf 7:29–39. https://doi.org/10.1007/s40964-021-00216-z
9. Rizza G, Galati M, Antonioni P, Iuliano L (2023) Effect of the sintering conditions on the neck growth during the powder bed

fusion with electron beam (PBF-EB) process. J Manuf Mater Process 7:55. https://doi.org/10.3390/jmmp7020055
10. Sakac I, Tropsa V, Sercer M, Solic S (2024) Influence of the LPBF process parameters on the porosity of the AlSi10Mg alloy. Tehnički Glasnik. 18(1). https://doi.org/10.31803/tg-20231206200048
11. Gao B, Zhao H, Peng L, Sun Z (2023) A review of research progress in selective laser melting (SLM). Micromachines 14(1):57. https://doi.org/10.3390/mi14010057
12. Ashwath P, Anthony XM, Jeyapandiarajan P, Joel J, Batako A (2022) Surface finish and property evaluation of direct metal laser sintered (DMLS) Al-Si-10Mg alloy. J Physics: Conference Series, Ser 2198:012055. https://doi.org/10.1088/1742-6596/2198/1/012055
13. Çelik A, Tekoğlu E, Yasa E, Sönmez MŞ (2022) Contact-free support structures for the direct metal laser melting process. Materials 15(11):3765. https://doi.org/10.3390/ma15113765
14. Shah A, Aliyev R, Zeidler H, Krinke S (2023) A review of the recent developments and challenges in wire arc additive manufacturing (WAAM) process. J Manuf Mater Process 7(3):97. https://doi.org/10.3390/jmmp7030097
15. Elementum—an inside look at how AM aluminium alloys are possible using RAM technology. https://www.elementum3d.com/white-papers/an-inside-look-at-how-am-commercial-aluminum-alloys-are-made-possible-using-ram-technology/. Accessed 5 June 2024
16. Migal – Wire Arc Additive Manufacturing (WAAM). https://migal.co/en/waam. Accessed 5 June 2023
17. Griffths D, Xu L, Gittos M, Allison A, Addison A (2020) High levels of porosity in TIG welds made between additively manufactured aluminium components. welding and cutting. Issue 2. https://www.welding-and-cutting.info/issues/issue-2-2020. Accessed 5 June 2024
18. Zhang C, Bao Y, Zhu H, Nie X, Zhang W, Zhang S, Zeng X (2019) A full comparison between Laser and TIG welding of selective laser melted AlSi10Mg. Optics Laser Technol. 120. https://doi.org/10.1016/j.optlastec.2019.105696
19. Gill M, Terry E, Abdi Y, Hawkes S, Rindler J, Schick D, Ramirez A, Herderick ED (2020) Joining technologies for metal additive manufacturing in the energy industry. Minerals, Metals Mater Soc. 72(12). https://doi.org/10.1007/s11837-020-04441-9
20. Emmelmann C, Beckmann F (2015) Hybrid lightweight design by laser additive manufacturing and laser welding process. Laser In Manufacturing Conference
21. Biffi C. A., Fiocchi J., Tuissi A (2019) Laser weldability of AlSi10Mg alloy produced by selective laser melting: microstructure and mechanical behavior. J Mater Eng Perform. 28(11). https://doi.org/10.1007/s11665-019-04402-7
22. Emmelmann C, Beckmann F (2017) Optimization of laser welding process for laser additive manufactured aluminum parts by means of beam oscillation and process-oriented component design. Laser In Manufacturing Conference
23. Cui L, Peng Z, Chang Y, He D, Cao Q, Guo X, Zeng Y (2022) Porosity, microstructure and mechanical property of welded joints produced by different laser welding processes in selective Laser melting AlSi10Mg alloys. Optics Laser Technol. 150. https://doi.org/10.1016/j.optlastec.2022.107952
24. Peng Z, Cui L, He D, Guo X, Zeng Y, Cao Q, Hang H (2022) Effect of Er and Zr addition on laser weldability of AlSi10Mg alloys fabricated by selective Laser melting. Mater Characterization. 190. https://doi.org/10.1016/j.matchar.2022.112070
25. Otten C, Gerhards B, Schleser M, Schwarz A, Gebhardt A (2022) Innovative Laserschweisstechnologie fur Additiv Gefertigde Bauteile. DVS Congress
26. Schwarz A, Schleser M, Gerhards B, Popoola P, Gebhardt A (2021) Welding of additive manufactured AlSi10Mg: using laser welding in a vacuum for high quality weld seams—a new approach to welding LPBF manufactured AlSi10Mg. South African J Industrial Eng. 32(4). https://doi.org/10.7166/32-4-2513
27. Chen N, Wan Z, Wang H, Li J, Yang B, Solomon J, Carlson B (2022) Effect of ambient pressure on Laser welding of AlSi10Mg fabricated by selected laser melting. Materials & Design. 215. https://doi.org/10.1016/j.matdes.2022.110427
28. Makikangas J, Rautio T, Mustakangas A, Mantyjarvi K (2019) Laser welding of AlSi10Mg aluminium-based alloy produced by selective laser melting (SLM). 17th Nordic Laser Mater Processing Conference (NOLAMPI17). https://doi.org/10.1016/j.promfg.2019.08.013
29. Dimatteo V, Liverani E, Ascari A, Fortunato A (2022) Weldability and mechanical properties of dissimilar laser welded aluminium alloys thin sheets produced by conventional rolling and additive manufacturing. J Mater Processing Technol. 302. https://doi.org/10.7166/32-4-2513
30. Möller B, Schnabel K, Wagener R, Kaufmann H, Melz T (2020) Fatigue assessment of additively manufactured AlSi10Mg laser beam welded to rolled EN AW-6082-T6 sheet metal. Int J Fatigue. 140. https://doi.org/10.1016/j.ijfatigue.2020.105805
31. Nahmany M, Rosenthal I, Benishti I, Frage N, Stern A (2015) Electron beam welding of AlSi10Mg workpieces produced by selectedLaser melting additive manufacturing technology. Additive Manufacturing. 8. https://doi.org/10.1016/j.addma.2015.08.002
32. Nahmany M, Stern A, Aghion E, Frage N (2017) Structural properties of EB-welded AlSi10Mg thin-walled pressure vessels produced by AM-SLM technology. J Mater Eng Perform. 26(10). https://doi.org/10.1007/s11665-017-2953-7
33. Nahmany M, Hadad Y, Aghion E, Stern A, Frage N (2019) Microstructural assessment and mechanical properties of electron beam welding of AlSi10Mg specimens fabricated by selective laser melting. J Mater Processing Technol. 270. https://doi.org/10.1016/j.jmatprotec.2019.02.025
34. Beckmann F, Emmelmann C (2019) Optimization of the weldability of laser additive manufactured aluminum by means of hydrogen minimization in the component and welding parameter optimization. Laser In Manufacturing Conference
35. Nunes R, Faes K, De Waele W, Simar A, Verlinde W, Lezaack M, Sneyers W, Arnhold J (2023) A review on the weldability of additively manufactured aluminium parts by fusion and solid-state welding processes. Metal. 13(10). https://doi.org/10.3390/met13101724
36. ISO 9015–1:2001. Destructive tests on welds in metallic materials — hardness testing. Part 1: hardness test on arc welded joints. https://www.iso.org/standard/32821.html. Accessed 5 Oct 2024
37. ISO 15614–2:2005. Specification and qualification of welding procedures for metallic materials — welding procedure test. Part 2: Arc welding of aluminium and its alloys. https://www.iso.org/standard/28408.html. Accessed 5 Oct 2024
38. Huangfu B, Liu Y, Liu X, Wu X, Bai H (2024) Anisotropy of additively manufactured metallic materials. Materials. 17. https://doi.org/10.3390/ma17153653
39. Liu Y, Liu Z, Zhou G, He C, Zhang J (2022) Microstructures and properties of Al-Mg alloys manufactured by WAAM-CMT. Mater. 15. https://doi.org/10.3390/ma15155460
40. Wang J, Zhu K, Zhang W, Zhu X, Lu X (2023) Microstructural and defect evolution during WAAM resulting in mechanical property differences for AA5356 component. J Market Res 22:982–996. https://doi.org/10.1016/j.jmrt.2022.11.116
41. Wu D, Cui L, Wu X, Guo X, Shao W, Tan Z, He D (2022) Cold metal transfer welding of AlSi7Mg alloy sheets prepared by selective laser melting. J Manuf Process 84(1):282–297. https://doi.org/10.1016/j.jmapro.2022.10.013

42. Ibrahim M, Abdelaziz M, Samuel A, Doty H, Samuel F (2021) Spheroidization and coarsening of eutectic Si particles in Ai-Si-based alloys. Adv Mater Sci Eng. https://doi.org/10.1155/2021/6678280
43. Scherillo F, Astarita A, Prisco R, Contaldi V, di Petta P, Langella A, Squillace A (2018) Friction stir welding of AlSi10Mg plates produced by selective laser melting. Metall, Microstructure Anal 7:457–463. https://doi.org/10.1007/s13632-018-0465-y
44. Abu Bakar SSS, Sharif S, Faridh M (2019) Assessment of friction stir welding on aluminium 3D printing materials. Int J Recent Technol Eng. 8(4). https://doi.org/10.1007/s40194-018-0585-7
45. Moeini G, Sajadifar SV, Wegener T, Brenne F, Niendorf T, Bohm S (2019) On the low-cycle fatigue behavior of friction stir welded Al–Si12 parts produced by selective laser melting. Mater Sci Eng A. 764. https://doi.org/10.1016/j.msea.2019.138189
46. Minhas N, Sharma V, Bhadauria SS (2023) Enhancing the properties of friction stir welded joints of L-PBF printed AlSi10Mg alloy via multi-variable optimization. Arch Civil Mechan Eng. https://doi.org/10.1007/s43452-022-00601-7
47. Thakur A, Mehlwal S, Minhas N, Sharma V (2022) Influence of tool rotational speed on the microstructural characterization and mechanical properties of friction stir welded Al-Si10Mg parts produced by DMLS additive manufacturing process. Mater Sci Eng B. 278. https://doi.org/10.1016/j.mseb.2022.115612
48. Thakur A, Sharma V, Minhas N, Manda S, Sharma VS (2023) Microstructure and mechanical properties of dissimilar friction stir welded joints of laser powder bed fusion processed AlSi10Mg and conventional hot rolled 6061-T6 thin sheet. Optics Laser Technol. 163. https://doi.org/10.1016/j.optlastec.2023.109382
49. El Hassanin A, Velotti C, Scherillo F, Astarita A, Squillace A, Carrino L (2017) Study of the solid state joining of additive manufactured components. IEEE 3rd Int Forum Res Technol Soc Industry (RTSI). https://doi.org/10.1109/RTSI.2017.8065967
50. Du Z, Tan MJ, Chen H, Bi G, Chua CK (2018) Joining of 3D-printed AlSi10Mg by friction stir welding. Welding in the World 63:675–682. https://doi.org/10.1007/s40194-018-0585-7
51. Zhou S., Wu K. Yang G., Wu B., Qin L., Guo X (2023) Friction stir welding of wire arc additively manufactured 205A aluminum alloy: microstructure and mechanical properties. Mater Sci Eng A. 876. https://doi.org/10.1016/j.msea.2023.145154
52. Mirandola P, Lunetto V, Novel D, Barozzi M, Bellutti P, De Maddis M, Spena PR (2023) Strength and microstructure of friction stir welded additively manufactured Scalmalloy® is As-welded and heat-treated conditions. J Manufact Processes. 97. https://doi.org/10.1016/j.jmapro.2023.04.051
53. Rajan ANR, Krochmal M, Wegener T, Hartmaier A, Niendorf T, Moeini G (2024) Micro-macro modeling of tensile behavior of a friction stir welded hybrid joint of AlSi10Mg parts produced by powder bed fusion and casting. Welding in the World 68:1693–1705. https://doi.org/10.1007/s40194-024-01775-9
54. Chatha JS, Bedi TS, Handa A (2019) Rotary friction welding of dissimilar materials. Int J Recent Int J Recent Technol Eng. 8. https://doi.org/10.35940/ijrte.D7456.118419
55. Murugan SS, Sathiya P, Haq AN (2021) Rotary friction welding and dissimilar metal joining of aluminium and stainless-steel alloys. Annals of "Dunarea de Jos" University of Galati. https://doi.org/10.35219/awet.2021.11
56. Lashari HR, Li S, Kong C, Asnavandi M, Zangeneh S (2021) Rotary friction welding of additively manufactured 17–4PH stainless steel. J Manufacturing Processes V 64:1517–1528. https://doi.org/10.1016/j.jmapro.2021.03.008
57. Balasz B, Bieleck M, Gulbinski W, Sloboda L (2023) Comparison of ultrasonic and other atomization methods in metal powder production. J Achievements Mater Manufacturing Eng. 116. https://doi.org/10.5604/01.3001.0016.3393
58. Fedina T, Belelli F, Lupi G, Branday B, Casati R, Berneth R, Brueckner F, Kaplan AFH (2022) Influence of AlSi10Mg powder aging on the material degradation and its processing in laser powder bed fusion. Powder Technology. 412. https://doi.org/10.1016/j.powtec.2022.118024